DOI:10.1021/ic900331m

Inorganic Chemistry
Article

Copper Phthalate Coordination Polymers Incorporating Kinked Dipyridyl Ligands: An Unprecedented 8-Connected Network and One-Dimensional Chiral Nanobarrels with Hydrophobic Channels Constructed from Septuple Helical Motifs

Maxwell A. Braverman,[†] Joseph H. Nettleman,[†] Ronald M. Supkowski,[‡] and Robert L. LaDuca*[,†]

[†]*Lyman Briggs College and Department of Chemistry, Michigan State University, East Lansing, Michigan 48825 and* [‡]*Department of Chemistry and Physics, King's College, Wilkes-Barre, Pennsylvania 18711*

Received February 18, 2009

Copper phthalate coordination polymers incorporating the kinked and hydrogen-bonding-capable imines 4,4′-dipyridylketone (dpk) and 4,4′-dipyridylamine (dpa) have been prepared and structurally characterized by single-crystal X-ray diffraction. $\{[Cu(pht)(dpk)]\cdot 0.33CH_3OH\}_n$ (**1**; pht = phthalate) possesses helical subunits built from the fusion of $[Cu(dpk)]_n$ 3-fold double helices and $[Cu(pht)]_n$ 3-fold helices with opposite handedness. The resulting achiral $[Cu(pht)(dpk)]_n$ helices are conjoined by bridging phthalate carboxylate oxygen atoms to construct $\{Cu_2O_2\}$ dimeric units, which serve as 8-connected nodes for a three-dimensional (3D) coordination polymer lattice with an unprecedented $3^6 4^{12} 5^8 6^2$ topology, evocative of a 3D Kagome lattice. $\{[Cu_2(pht)_2(dpa)]\cdot H_2O\}_n$ (**2**) manifests homochiral septuple left-handed $[Cu_2O_2(dpa)]_n$ helices formed by copper ions, phthalate oxygen atoms, and dpa ligands. The septuple helices are bracketed by pht anions to construct chiral one-dimensional nanobarrels with solvent-free "star-shaped" channels. Compounds **1** and **2** display antiferromagnetic [$J = -9.85(5)$ cm^{-1}] and ferromagnetic [$J = +1.36(3)$ cm^{-1}] coupling across their $\{Cu_2O_2\}$ dimeric units, respectively.

Introduction

Metal−organic framework materials (MOFs) remain a popular research focus not only because of their potential utility in hydrogen storage,[1] shape-selective separations,[2] ion exchange,[3] catalysis,[4] and optical devices[5] but also because of the innate aesthetic appeal of their often elegant molecular structures.[6] Benzenedicarboxylate and benzenetricarboxylate ligands are the most common connectors used for linking cationic metal nodes because they provide a rigid structural scaffolding along with the charge balance required to foster neutral frameworks that lack porosity-inhibiting anions. Neutral dipyridyl coligands such as 4,4′-bipyridine (4,4′-bpy) have been employed in tandem with benzenedicarboxylate ligands to promote structural variability and expand the scope of useful MOF properties. For example, the interpenetrated three-dimensional (3D) material [Zn(terephthalate)(4,4′-bpy)$_{0.5}$] can serve as a stationary phase for the chromatographic separation of branched and linear hydrocarbons.[7]

*To whom correspondence should be addressed. E-mail: laduca@msu.edu.

(1) (a) Li, H.; Eddaoudi, M.; O'Keeffe, M.; Yaghi, O. M. *Nature (London)* **2005**, *402*, 276–279. (b) Matsuda, R.; Kitaura, R.; Kitagawa, S.; Kubota, Y.; Belosludov, R. U.; Kobayashi, T. C.; Sakamoto, H.; Chiba, T.; Takata, M.; Kawazoe, Y.; Mita, Y. *Nature (London)* **2005**, *436*, 238–241. (c) Pan, L.; Holson, D.; Ciemnolonski, L. R.; Heddy, R.; Li, J. *Angew. Chem., Int. Ed.* **2006**, *46*, 616–619. (d) Rosi, N. L.; Eckert, J.; Eddaoudi, M.; Vodak, D. J.; Kim, J.; O'Keeffe, M.; Yaghi, O. M. *Science* **2003**, *300*, 1127–1129. (e) Dinca, M.; Yu, A. F.; Long, J. R. *J. Am. Chem. Soc.* **2006**, *128*, 8904–8913. (f) Ferey, G.; Latroche, M.; Serre, C.; Millange, F.; Loiseau, T.; Percheron-Guegan, A. *Chem. Commun.* **2003**, 2976–2977.

(2) (a) Seo, J. S.; Whang, D.; Lee, H.; Jun, S. I.; Oh, J.; Jeon, Y. J.; Kim, K. *Nature (London)* **2000**, *404*, 982–986. (b) Cingolani, A.; Galli, S.; Masciocchi, N.; Pandolfo, L.; Pettinari, C.; Sironi, A. *J. Am. Chem. Soc.* **2005**, *127*, 6144–6145.

(3) (a) Fang, Q.-R.; Zhu, G.-S.; Xue, M.; Sun, J.-Y.; Qiu, S.-L. *Dalton Trans.* **2006**, 2399–2402. (b) Zhang, X.-M.; Tong, M.-L.; Lee, H. K.; Chen, X.-M. *J. Solid State Chem.* **2001**, *160*, 118–122. (c) Yaghi, O. M.; Li, H.; Groy, T. L. *Inorg. Chem.* **1997**, *36*, 4292–4293.

(4) (a) Guillou, N.; Forster, P. M.; Gao, Q.; Chang, J. S.; Nogues, M.; Park, S.-E.; Cheetham, A. K.; Ferey, G. *Angew. Chem., Int. Ed.* **2001**, *40*, 2831–2834. (b) Wu, C.-D.; Hu, A.; Zhang, L.; Lin, W. *J. Am. Chem. Soc.* **2005**, *127*, 8940–8941. (c) Han, H.; Zhang, S.; Hou, H.; Fan, Y.; Zhu, Y. *Eur. J. Inorg. Chem.* **2006**, *8*, 1594–1600. (d) Mori, W.; Takamizawa, S.; Kato, C. N.; Ohmura, T.; Sato, T. *Microporous Mesoporous Mater.* **2004**, *73*, 15–30. (e) Baca, S. G.; Reetz, M. T.; Goddard, R.; Filippova, I. G.; Simonov, Y. A.; Gdaniec, M.; Gerbeleu, N. *Polyhedron* **2006**, *25*, 1215–1222.

(5) (a) Zang, S.; Su, Y; Li, Y.; Ni, Z.; Meng, Q. *Inorg. Chem.* **2006**, *45*, 174–180. (b) Wang, L.; Yang, M.; Li, G.; Shi, Z.; Feng, S. *Inorg. Chem.* **2006**, *45*, 2474–2478. (c) Wang, S.; Hou, Y.; Wang, E.; Li, Y.; Xu, L.; Peng, J.; Liu, S.; Hu, C. *New J. Chem.* **2003**, *27*, 1144–1147. (d) Beauvais, L. G.; Shores, M. P.; Long, J. R. *J. Am. Chem. Soc.* **2000**, *122*, 2763–2772. (e) Jianghua, H.; Jihong, Y.; Yuetao, Z.; Qinhe, P.; Ruren, X. *Inorg. Chem.* **2005**, *44*, 9279–9282. (f) Lu, W.-G.; Su, C.-Y.; Lu, T.-B.; Jiang, L.; Chen, J.-M. *J. Am. Chem. Soc.* **2006**, *128*, 34–35. (g) Qin, C.; Wang, X.-L.; Li, Y.-G.; Wang, E.-B.; Su, Z.-M.; Xu, L.; Clerac, R. *Dalton Trans.* **2005**, 2609–2614.

(6) (a) Cheetham, A. K.; Rao, C. N. R.; Feller, R. K.; Blatov, V. A.; Carlucci, L.; Ciani, G.; Proserpio, D. M. *Chem. Commun.* **2006**, *6*, 4780–4795 and references cited therein. (b) Blatov, V. A.; Carlucci, L.; Ciani, G.; Proserpio, D. M. *CrystEngComm* **2004**, *6*, 377–395 and references cited therein.

(7) Chen, B.; Liang, C.; Yang, J.; Contreras, D. S.; Clancy, Y. L.; Lobkovsky, E. B.; Yaghi, O. M.; Dai, S. *Angew. Chem., Int. Ed.* **2006**, *45*, 1390–1393.

Published on Web 4/21/2009

Scheme 1

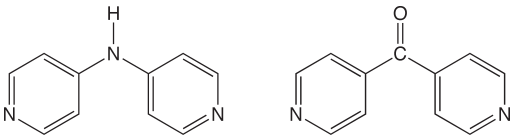

Recently, our group has been exploring the synthesis and characterization of divalent metal dicarboxylate coordination polymers containing the organodiimine 4,4′-dipyridylamine (dpa; Scheme 1).[8] In contrast to the rigid-rod tether 4,4′-bpy, dpa possesses a kinked orientation of its distal nitrogen donor atoms in addition to a hydrogen-bonding point of contact at its central amine functional group. Our previous investigations have shown that the specific covalent and supramolecular interactions provided by dpa ligands can promote the self-assembly of MOFs with intriguing structural topologies.[9−12] $\{[Cu(succinate)(dpa)]\cdot 0.5H_2O\}_n$ adopts a relatively uncommon doubly interpenetrated $CdSO_4$ structure type ($6^5 8$ topology), constructed from the intersection of $[Cu(dpa)]_n^{2n+}$ 4-fold double helices by orthogonal sets of parallel $[Cu(suc)]_n$ linear one-dimensional (1D) chain motifs.[9] $\{[Ni(dpa)_2(succinate)_{0.5}]Cl\}$ exhibits a unique 5-connected self-penetrated structure with a uniform 6^{10} topology, formed from the covalent linkage of 4-fold interpenetrated $[Ni(dpa)_2]_n^{2n+}$ cationic diamondoid sublattices by succinate bridging ligands.[9] $[Ni(adipate)(dpa)(H_2O)]_n$ represented the first reported example of a 3-fold interpenetrated PtS lattice ($4^2 8^4$ topology).[10] In contrast to dpa, the coordination polymer chemistry of the related 4,4′-dipyridylketone (dpk; Scheme 1) remains largely undeveloped,[13] despite its successful employment in the construction of palladium-based molecular hexagons.[14]

Herein we report two topologically unique divalent copper phthalate coordination polymers containing these kinked and hydrogen-bonding-capable dipyridines, $\{[Cu(pht)(dpk)]\cdot 0.33CH_3OH\}_n$ (**1**; pht = phthalate) and $\{[Cu_2(pht)_2(dpa)]\cdot H_2O\}_n$ (**2**). Complex **1** represents a novel, striking 8-connected, 3D coordination polymer lattice built from achiral helical subunits. On the other hand, the smaller steric hindrance imparted by the amine functional groups of the dipyridyl ligands in **2** affords coordination polymer nanobarrels with solvent-free 1D channels, constructed from intriguing chiral septuple helical submotifs. In addition, divergent variable-temperature magnetic behavior is observed in these materials.

Experimental Section

General Considerations. Copper salts were obtained commercially from Fisher. 4,4′-Dipyridylketone (dpk) was prepared via the reaction of 4-lithiopyridine and ethyl isonicotinate in a modification of Chen and Mak's procedure for the synthesis of 3,3′-dipyridylketone.[15] 4,4′-Dipyridylamine (dpa) was prepared by a published procedure.[8] Water was deionized above 3 MΩ-cm in-house. Thermogravimetric analysis (TGA) was performed on a TA Instruments TGA 2050 thermogravimetric analyzer with a heating rate of 10 °C/min up to 600 °C. Elemental analysis was carried out using a Perkin-Elmer 2400 series II CHNS/O analyzer. IR spectra were recorded on a Perkin-Elmer Spectrum One instrument on ground powdered samples. Variable-temperature magnetic susceptibility data (2−300 K) for **1** and **2** were collected on a Quantum Design MPMS SQUID magnetometer at an applied field of 0.1 T. After each temperature change, the sample was kept at the new temperature for 5 min before magnetization measurement to ensure thermal equilibrium. The susceptibility data were corrected for paired electron diamagnetism using Pascal's constants[16] and also for the diamagnetism of the sample container.

Preparation of $\{[Cu(pht)(dpk)]\cdot 0.33CH_3OH\}_n$ (1). A mixture of hydrated copper nitrate (90 mg, 0.37 mmol) and phthalic acid (62 mg, 0.37 mmol) was dissolved in 3 mL of water in a 15 mL test tube. A 1 mL aliquot of a 1:1 water/methanol solution was layered carefully on top. A solution containing dpk (68 mg, 0.37 mmol) in 3 mL of methanol was then layered on top. Blue crystals of **1** (67 mg, 43% yield based on Cu) were isolated after allowing the tube to sit undisturbed for 2 weeks, followed by filtration, washing with distilled water, ethanol, and acetone, and drying in air. Anal. Calcd for $C_{19.33}H_{13.33}CuN_2O_{5.33}$: C, 54.96; H, 3.18; N, 6.63. Found: C, 54.27; H, 3.16; N, 6.40. IR (ν/cm^{-1}): 3109 w, 1741 w, 1672 m, 1624 s, 1594 m, 1574 s, 1551 w, 1491 w, 1445 w, 1417 m, 1365 s, 1349 s, 1334 s, 1274 m, 1219 w, 1141 w, 1084 w, 1067 w, 1059 w, 1038 w, 1020 w, 980 w, 955 w, 866 w, 843 m, 833 m, 819 w, 788 w, 766 s, 717 m, 704 m, 693 m, 616 w.

Preparation of $\{[Cu_2(pht)_2(dpa)]\cdot H_2O\}_n$ (2). A mixture of $CuCl_2\cdot 2H_2O$ (63 mg, 0.37 mmol), potassium hydrogen phthalate (76 mg, 0.37 mmol), and dpa (48 mg, 0.28 mmol) was suspended in 6 g of H_2O (333 mmol) in a borosilicate glass tube that had been flame-sealed at one end. The tube was then flame-sealed and heated at 120 °C for 24 h. Long green hexagonal needles of **2** (54 mg, 45% yield based on Cu) were isolated by filtration, washed with distilled water, ethanol, and acetone, and dried in air. Anal. Calcd for $C_{26}H_{19}Cu_2N_3O_9$: C, 48.45; H, 2.97; N, 6.52. Found: C, 47.99; H, 2.77; N, 6.42. IR (ν/cm^{-1}): 3491 m br, 3396 m br, 1657 m, 1607 s, 1531 s, 1508 s, 1427 m, 1389 m, 1358 s, 1220 m, 1152 w, 1086 w, 1067 w, 1033 w, 918 w, 880 w, 826 m, 769 w, 719 w, 665 w, 615 w.

X-ray Crystallography. Single-crystal X-ray diffraction data for a blue block of **1** (with dimensions 0.24 mm × 0.16 mm × 0.06 mm) and a green needle of **2** (with dimensions 0.80 mm × 0.14 mm × 0.12 mm) were collected using a Bruker-AXS SMART 1K CCD instrument at 173(2) K. Reflection data were acquired using graphite-monochromated Mo Kα radiation (λ = 0.710 73 Å). The data were integrated via *SAINT*.[17] Lorentz and polarization effects and multiscan absorption corrections were applied with *SADABS*.[18] The structures were solved using direct methods and refined on F^2 using *SHELXTL*.[19] All non-hydrogen atoms were refined anisotropically. Hydrogen atoms bound to carbon atoms were placed in

(8) Zapf, P. J.; LaDuca, R. L.; Rarig, R. S., Jr.; Johnson, K. M., III; Zubieta, J. *Inorg. Chem.* **1998**, *37*, 3411–3414.
(9) Montney, M. R.; Mallika Krishnan, S.; Patel, N. M.; Supkowski R. M.; LaDuca, R. L. *Cryst. Growth Des.* **2007**, *7*, 1145–1153.
(10) Montney, M. R.; Mallika Krishnan, S.; Supkowski, R. M.; LaDuca, R. L. *Inorg. Chem.* **2007**, *46*, 7362–7370.
(11) Martin, D. P.; Supkowski, R. M.; LaDuca, R. L. *Inorg. Chem.* **2007**, *46*, 7917–7922.
(12) Braverman, M. A.; LaDuca, R. L. *CrystEngComm* **2008**, *10*, 117–124.
(13) Knapp, W. R.; Supkowski, R. M.; LaDuca, R. L. *Inorg. Chem. Commun.* **2008**, *11*, 1276–1279.
(14) Leininger, S.; Schmitz, M.; Stang, P. J. *Org. Lett.* **1999**, *1*, 1921–1923.
(15) Chen, X.-D.; Mak, T. C. W. *J. Mol. Struct.* **2005**, *743*, 1–6.
(16) Khan, O. *Molecular Magnetism*; VCH Publishers: New York, 1993.
(17) *SAINT, Software for Data Extraction and Reduction*, version 6.02; Bruker AXS, Inc.: Madison, WI, 2002.
(18) *SADABS, Software for Empirical Absorption Correction*, version 2.03; Bruker AXS, Inc.: Madison, WI, 2002.
(19) Sheldrick, G. M. *SHELXTL, Program for Crystal Structure Refinement*; University of Göttingen: Göttingen, Germany, 1997.

Table 1. Crystal and Structure Refinement Data for **1** and **2**

data	**1**	**2**
empirical formula	$C_{19.33}H_{13.33}CuN_2O_{5.33}$	$C_{26}H_{19}Cu_2N_3O_9$
fw	429.87	644.52
collection T (K)	173	173
λ (Å)	0.710 73	0.710 73
cryst syst	rhombohedral	hexagonal
space group	$R\bar{3}$	$P6_5$
a (Å), b (Å)	24.926(2)	27.590(3)
c (Å)	15.189(3)	5.9277(14)
V (Å^3)	8173.0(18)	3907.7(11)
Z	18	6
D_{calc} (g cm^{-3})	1.565	1.643
μ (mm^{-1})	1.242	1.692
min/max transmn	0.922	0.850
hkl ranges	$-32 \le h \le 32$, $-32 \le k \le 31$, $-19 \le l \le 20$	$-35 \le h \le 36$, $-36 \le k \le 36$, $-7 \le l \le 7$
total reflns	27 775	48 230
unique reflns	4010	6409
R(int)	0.0886	0.0589
param/restraints	262/1	370/5
R1[a] (all data)	0.0884	0.0575
R1[a] [$I > 2\sigma(I)$]	0.0443	0.0518
wR2[b] (all data)	0.1164	0.1255
wR2[b] [$I > 2\sigma(I)$]	0.1029	0.1227
max/min residual (e Å^{-3})	0.643/−0.466	0.871/−0.659
GOF	1.022	1.084

[a] $R1 = \sum||F_o| - |F_c||/\sum|F_o|$. [b] $wR2 = \{\sum[w(F_o^2 - F_c^2)^2]/\sum[wF_o^2]^2\}^{1/2}$.

calculated positions and refined isotropically with a riding model. The dpa amine hydrogen atom in **2** was found via Fourier difference maps and then restrained at fixed positions and refined isotropically. Relevant crystallographic data for **1** and **2** are listed in Table 1. Supramolecular contact information and incipient void-space volumes were computed with *PLATON* software.[20] Network topologies were calculated using the *TOPOS*[21] software suite.

Results and Discussion

Synthesis and IR Spectra. Compound **1** was prepared by the slow diffusion of an aqueous solution of copper nitrate and phthalic acid with a methanolic solution of dpk, while **2** was synthesized by the hydrothermal reaction of copper chloride, potassium hydrogen phthalate, and dpa. Their respective IR spectra corresponded with the structural elements ascertained by single-crystal X-ray diffraction.

Medium-intensity bands in the range of ∼1600−1200 cm^{-1} can be ascribed to stretching modes of the pyridyl rings of the dpa or dpk ligands and the aromatic rings of the pht ligands.[22] Puckering modes of the pyridyl and/or phenyl rings occurred in the region between 820 and 600 cm^{-1}. Asymmetric and symmetric C−O stretching modes of the fully deprotonated pht ligands correspond to the strong, broadened features at 1594 and 1350 cm^{-1} (for **1**) and 1574 and 1365 cm^{-1} (for **2**). The strong band at 1624 cm^{-1} in the spectrum of **1** is diagnostic for the C=O stretch of the ketone functional group of dpk. The absence of any bands in the region of 1700 cm^{-1} signifies full deprotonation of the pht ligands. Broadened yet weak bands in the region of ∼3500−3400 cm^{-1} indicate N−H stretching modes within the dpa ligands and water molecules of crystallization in **2**; the broad feature at ∼3100 cm^{-1} in the spectrum of **1** is likely caused by O−H stretching modes within the cocrystallized methanol molecules.

Structural Description of 1. The asymmetric unit of compound **1** consists of one divalent copper atom, one pht dianion, one dpk molecule, and one unligated disordered methanol molecule (Figure 1). The coordination environment about copper is best described as a $\{CuO_3N_2\}$ distorted square pyramid, with an Addison and Rao trigonality factor of 0.14.[23] Pyridyl nitrogen donor atoms from two dpk ligands occupy two of the basal coordination sites in a trans orientation. Similarly, oxygen donor atoms from two pht ligands occupy the remaining two basal coordination sites in a trans disposition. The square-pyramidal coordination environment is completed by an oxygen donor atom from another pht ligand (O2), situated in the apical position. This atom bridges to a basal coordination site of a neighboring, symmetry-related copper atom, thus constructing a $\{Cu_2O_2\}$ dimeric unit. This kernel is defined by Cu···Cu and O···O through-space distances of 3.427 and 2.726 Å, respectively. Its geometry is rather pinched, with O−Cu−O and Cu−O−Cu angles measuring respectively 76.7 and 103.3°. Bond lengths and angles about the divalent copper atom in **1** are consistent with a Jahn−Teller-actived[9] electronic configuration ion (Table S1 in the Supporting Information).

Considering covalent connectivity only through the basal coordination sites, each copper atom connects to four others through two dpk and two pht ligands, thereby establishing $[Cu(pht)(dpk)]_n$ helical motifs oriented parallel to the c crystal direction (Figure 2). The Cu···Cu distances spanned by the dpk ligands within the helix are 11.378 Å, with the inter-ring torsion angle within the dpk ligand subtending an angle of 48.5°. This connectivity pattern forms $[Cu(dpk)]_n$ 3-fold double helices with a pitch of 30.378 Å (shown in green and blue in Figure 2), which are subsequently connected together by pht dianions to construct the overarching $[Cu(pht)(dpk)]_n$ helical motif. The Cu···Cu distances through the pht ligands measure 7.250 Å; the carboxylate groups of the pht dianions are twisted by 13.1 and 80.6° relative to the plane of the aromatic rings. Within a single overall helical motif is embedded a $[Cu(pht)]_n$ 3-fold helix (shown in orange in Figure 2); its pitch of 15.189 Å defines the c lattice parameter.

Moreover, the $[Cu(dpk)]_n$ 3-fold double helices and the $[Cu(pht)]_n$ 3-fold helix within a single $[Cu(pht)(dpk)]_n$ motif possess opposite handedness. In Figure 3, $[Cu(pht)(dpk)]_n$ helical patterns with embedded right-handed $[Cu(pht)]_n$ 3-fold helices and left-handed $[Cu(dpk)]_n$ 3-fold double helices are depicted in red, while those containing left-handed $[Cu(pht)]_n$ helices and right-handed $[Cu(dpk)]_n$ helices are shown in green. Adjacent $[Cu(pht)(dpk)]_n$ helical motifs thus have opposite handedness (Figure 3), resulting in an acentric crystal structure for **1**.

(20) Spek, A. L. *PLATON, A Multipurpose Crystallographic Tool*; Utrecht University: Utrecht, The Netherlands, 1998.
(21) Blatov, V. A.; Shevchenko, A. P.; Serezhkin, V. N. *J. Appl. Crystallogr.* **2000**, *33*, 1193, http://www.topos.ssu.samara.ru.
(22) Kurmoo, M.; Estournes, C.; Oka, Y.; Kumagai, H.; Inoue, K. *Inorg. Chem.* **2005**, *44*, 217–224.
(23) Addison, A. W.; Rao, T. N. J. *J. Chem. Soc., Dalton Trans.* **1984**, 1349–1356.

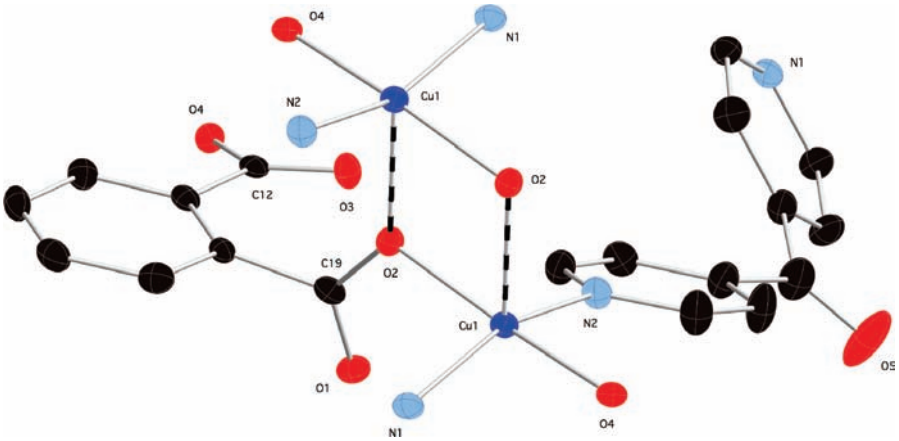

Figure 1. Coordination environment of **1** with thermal ellipsoids at 50% probability and a partial atom numbering scheme. The hydrogen atoms and the disordered cocrystallized methanol molecule are omitted. Long Cu−O bonds within the $\{Cu_2O_2\}$ dimeric unit are shown as dashed lines.

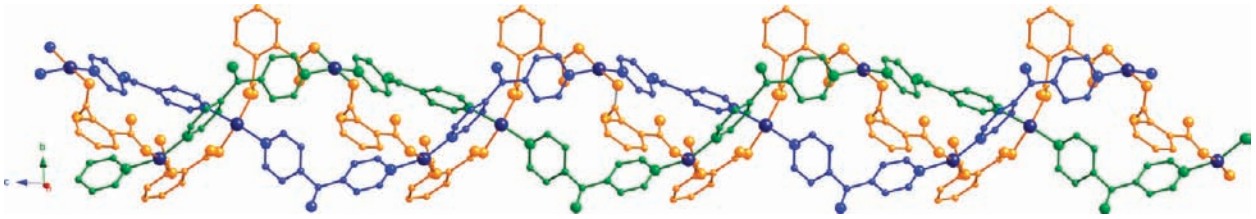

Figure 2. Side-on perspective of the $[Cu(pht)(dpk)]_n$ helical motif within the structure of **1**.

Through four pht and four dpa ligands, each dinuclear $\{Cu_2O_2\}$ unit is covalently connected to eight others, linking each $[Cu(pht)(dpk)]_n$ helix to three other helices, thereby constructing the overall 3D coordination polymer structure of **1**. Considering the centroids of the dinuclear units as connecting nodes, an 8-connected lattice with 3D $3^6 4^{12} 5^8 6^2$ topology can be constructed (Figure 4). Although this network is unprecedented in coordination polymer chemistry to the best of our knowledge, it has been predicted mathematically (as net *sqc876*) by the authors of the EPINET database of Euclidean patterns in non-Euclidean tilings.[24] Viewed from its side, the novel network of **1** visually resembles stacked Kagome lattices. Extraframework space within the structure of **1**, occupying 13.8% of the unit cell volume according to *PLATON*,[20] contains the disordered cocrystallized methanol molecules.

Structural Description of 2. Compound **2** crystallized in the acentric hexagonal space group $P6_5$, with a Flack parameter[25] of 0.010(15) indicating enantiomeric purity within the crystal. Although two other single crystals of **2** were also found to crystallize in the same space group, a racemic mixture of crystals with $P6_1$ and $P6_5$ in the bulk is still plausible. The asymmetric unit of **2** contains two divalent copper atoms, two pht dianions (pht-A, C21−C28/O1−O4; pht-B, C31−C38/O5−O8), one dpa molecule, and one water molecule of crystallization (Figure 5). The coordination environments at the crystallographically distinct copper atoms are virtually ideal $\{CuO_4N\}$ square pyramids with Addison and Rao τ factor values[23] of 0.003 and 0.005 for Cu1 and Cu2, respectively. Within the square-pyramidal coordination environment at Cu1, the basal plane is comprised of two oxygen donors from a chelating carboxylate group belonging to pht-B, a single oxygen atom from a carboxylate group belonging to pht-A, and a nitrogen donor atom from the dpa ligand. Occupying the apical site is another carboxylate oxygen atom, from a second pht-B ligand. The arrangement of donor atoms at Cu2 is similar, with two oxygen donors from a chelating carboxylate terminus of pht-A, a single oxygen donor atom from a carboxylate group of pht-B, and a pyridyl nitrogen atom from dpa filling the basal plane. A carboxylate oxygen atom from a second pht-A ligand is located at the apical site. Bond lengths and angles about the copper atoms in **2** are standard for Jahn−Teller-active d^9 configuration ions in square-pyramidal geometry with one chelating ligand (Table S2 in the Supporting Information).

As seen in Figure 5, adjacent Cu1 and Cu2 atoms are connected by μ_2-oxygen atoms from pht-A and pht-B ligands to form a pinched, virtually coplanar $\{Cu_2O_2\}$ dinuclear unit. The Cu···Cu and O···O distances across the metallacycle measure 3.380 and 2.602 Å, respectively, with Cu···O···Cu angles of 103.34(12) and 106.74(13)° and O···Cu···O angles of 74.45(11) and 75.47(11)°.

Individual $\{Cu_2O_2\}$ dinuclear kernels are strung into a 1D 6-fold left-handed $[Cu_2O_2(dpa)]_n$ helix with a pitch of 41.494 Å by linkage through the kinked dpa tethers (Figure S1 in the Supporting Information). The Cu···Cu interatomic distance bridged by the dpa ligands is 11.503 Å; the inter-ring torsion angle within the dpa ligands is 19.6°. The long pitch of a single $[Cu_2O_2(dpa)]_n$

(24) The EPINET database can be accessed at http://epinet.anu.edu.au.
(25) (a) Bernardinelli, G.; Flack, H. D. *Acta Crystallogr.* **1985**, *A41*, 500. (b) Flack, H. D. *Acta Crystallogr.* **1983**, *A29*, 876.

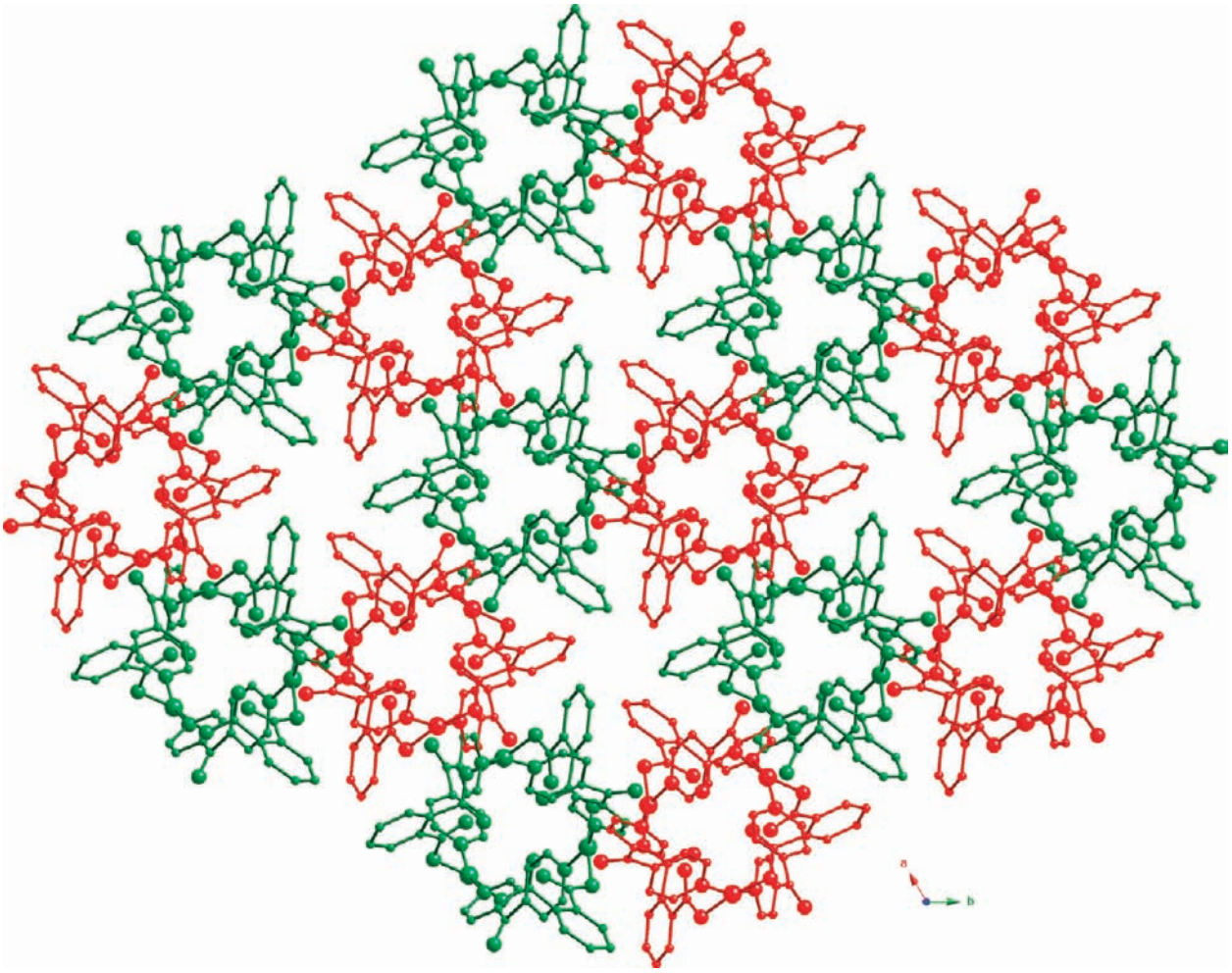

Figure 3. Arrangement of $[Cu(pht)(dpk)]_n$ helical motifs with alternating handedness in **1**.

helix allows the interleaving of six other left-handed $[Cu_2O_2(dpa)]_n$ helices, creating an intriguing homochiral septuple helix motif within the structure of **2** (Figure 6). The closest Cu···Cu interhelix contact distance is 5.928 Å, which defines the *c* lattice parameter.

Oxygen atoms (O1) within each $\{Cu_2O_2\}$ metallacycle in one $[Cu_2O_2(dpa)]_n$ helix and those within metallacycles in a second $[Cu_2O_2(dpa)]_n$ helix belong to the same exotridentate pht-A ligands that project into the interior of the septuple helix motif. Similarly, oxygen atoms (O5) within each $\{Cu_2O_2\}$ metallacycle and those belonging to a third $[Cu_2O_2(dpa)]_n$ helix are part of the same exotridentate pht-B ligands that are oriented toward the exterior of the septuple helix pattern. Thus, through both sets of bridging pht ligands, fully covalently connected 1D $[Cu_2(pht)_2(dpa)]_n$ homochiral nanobarrels are constructed within the structure of **2** (Figure 7). The closest interatomic distance within the interior of the nanobarrel, between hydrogen atoms of pht-A ligands, is 9.311 Å (neglecting van der Waals radii). The resulting 1D hydrophobic solvent-free "pinwheel"-shaped void space occupies 11.7% of the unit cell volume, as calculated by *PLATON*.[20] Taking atomic van der Waals radii[26] into account, it can be estimated that 1D solvent-free "star-shaped" voids are approximately 7 Å across. Chiral nanotubular coordination polymers constructed from helical subunits are extremely rare,[27] with the octuple helical subunits in $\{[(CH_3)_2NH_2][Cd(4,4'\text{-biphenyldicarboxylate})_{1.5}]\cdot 2DMA\}_n$ currently holding the record for the highest level of intertwined helices in this class of materials.[27] The hydrophobic aromatic rings of the pht ligands projecting into the nanobarrel interior in **2** likely prevent the occlusion of any water molecules within the nanobarrels.

The nanobarrel motifs in **2** dramatically contrast with the undulating $[M(H_2O)_4(dpa)M(pht)_2(dpa)]_n$ (M = Co, Ni) 1D chains seen in cobalt and nickel coordination polymers incorporating the same two organic components, in which the metal ions display octahedral coordination spheres.[28] A further contrast exists between **2** and its 4,4′-bpy congener $\{[Cu(pht)(4,4'\text{-bpy})(H_2O)_2]\cdot 2H_2O\}_n$,[29] which forms a standard (4,4) grid layer coordination polymer motif that lacks any multinuclear units.

If each $\{Cu_2O_2\}$ metallacycle is treated as a 4-connected node, joined to two others within a single $[Cu_2O_2(dpa)]_n$ helix by dpa ligands and to two others in neighboring

(26) Shannon, R. D. *Acta Crystallogr.* **1976**, *A32*, 751–767.

(27) (a) Hao, X. R.; Wang, X. L.; Qin, C.; Su, Z. M.; Wang, E. B.; Lan, Y. Q.; Shao, K. Z. *Chem. Commun.* **2007**, 4620–4622. (b) Orr, G. W.; Barbour, L. J.; Atwood, J. L. *Science* **1999**, *285*, 1049–1052. (c) Cui, Y.; Lee, S. J.; Lin, W. *J. Am. Chem. Soc.* **2003**, *125*, 6014–6015.

(28) Braverman, M. A.; Supkowski, R. M.; LaDuca, R. L. *Inorg. Chim. Acta* **2007**, *360*, 2353–2362.

(29) Xu, H.; Sun, R.; Li, Y.-Z.; Bai, J.-F. *Acta Crystallogr.* **2006**, *E62*, m1156–m1158.

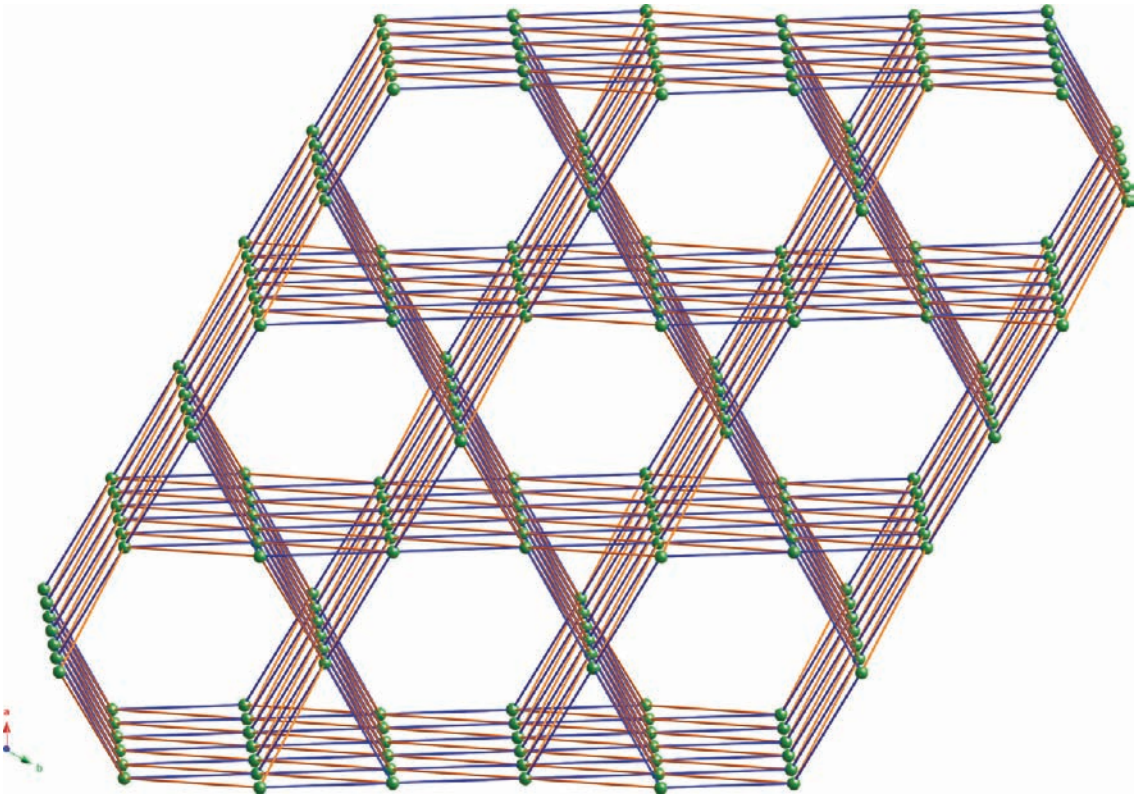

Figure 4. $3^6 4^{12} 5^8 6^2$ topology, 8-connected, 3D coordination polymer network of **1**. The spheres represent the centroids of the $\{Cu_2O_2\}$ dinuclear units. Blue and orange sticks represent the pht and dpk ligands, respectively.

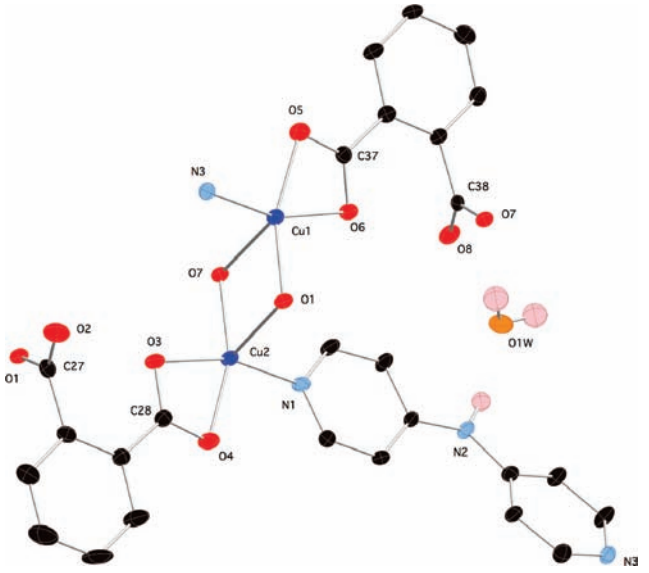

Figure 5. Coordination environment of **2**. Thermal ellipsoids are shown at 50% probability. Most hydrogen atoms have been omitted.

$[Cu_2O_2(dpa)]_n$ helices via pht bridges, the resulting topology can be viewed as a (4,4) sheet twisted and then folded over and spliced to itself (Figure S2 in the Supporting Information). The Schäfli symbol for the 4-connected 1D nanotubular network in **2** is $4^4 6^2$, with a long vertex symbol of $4.4.4.4.6_2.6_2$, as calculated by *TOPOS* software.[21]

The 1D $[Cu_2(pht)_2(dpa)]_n$ homochiral nanobarrels aggregate together via hydrogen-bonding interactions promoted by water molecules of crystallization that lie between the nanobarrel motifs. These water molecules are anchored to the exterior of the nanobarrel to accept hydrogen bonds from dpa amine groups projecting out of one nanobarrel and donate hydrogen bonds to unligated pht-B and pht-A carboxylate oxygen atoms situated on the periphery of another nanobarrel (Figure 7). Geometric parameters for these supramolecular interactions are given in Table S3 in the Supporting Information. The closest approach distance (27.590 Å) between the central cavities of adjacent chiral nanobarrels marks both the *a* and *b* lattice parameters.

Magnetic Properties. Variable-temperature magnetic susceptibility measurements were undertaken in order to examine possible spin communication across the $\{Cu_2O_2\}$ subunits in both **1** and **2**. Magnetic data for both compounds were fit acceptably to the Curie–Weiss law. For **1**, the best fit of the χ_m^{-1} vs T data gave $C = 0.41$ cm^3 K^{-1} mol^{-1} and $\theta = -4.02$ K, marking likely antiferromagnetic coupling across its $\{Cu_2O_2\}$ dimers. On the other hand, apparent ferromagnetic coupling is evident in **2**, with $C = 0.41$ cm^3 K^{-1} mol^{-1} and $\theta = +1.46$ K.

The variable-temperature magnetic data for **1** were fit with the standard Bleaney–Bowers[30] equation (eq 1) for an interacting pair of $S = {}^1/_2$ ions. Nonlinear regression gave $g = 2.093(2)$ and $J = -9.85(5)$ cm^{-1} with $R = 1.5 \times 10^{-5} = \{\sum[(\chi_m T)_{obs} - (\chi_m T)_{calc}]^2 / \sum[(\chi_m T)_{obs}]^2\}^{1/2}$ (Figure 8). The negative J value corroborates the singlet ground state and the antiferromagnetic coupling indicated by the Curie–Weiss treatment. The variable-tem-

(30) Bleaney, B.; Bowers, K. D. *Proc. R. Soc. London, Ser. A.* **1952** *214*, 451.

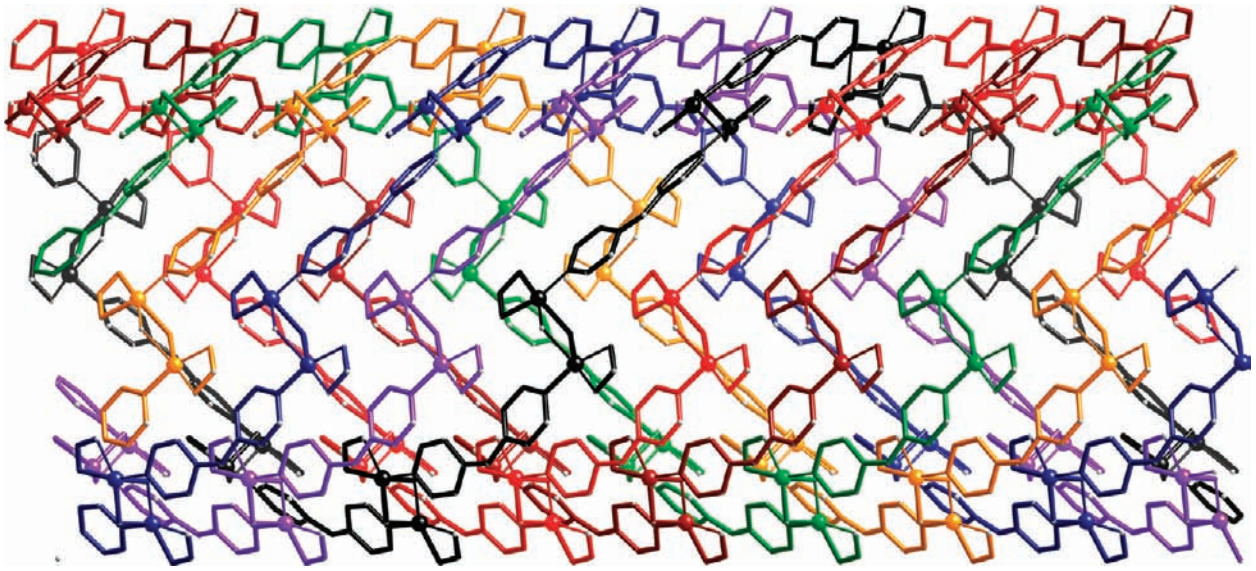

Figure 6. Homochiral $[Cu_2O_2(dpa)]_n$ septuple helix motif in **2**. Each of the seven helices is illustrated in a different color for clarity.

perature magnetic data for **2** were also fit with eq 1. Regression analysis gave $g = 2.098(1)$ and $J = +1.36(3)\,cm^{-1}$ with $R = 6.3 \times 10^{-6}$ (Figure 9). Thus, in contrast to **1**, **2** exhibits weak ferromagnetic superexchange across its $\{Cu_2O_2\}$ kernels.

Although both **1** and **2** possess equatorial−apical bridging across their respective $\{Cu_2O_2\}$ dinuclear units, subtle geometric differences within the square pyramidal coordination sphere can result in changes in magnetic behavior.[31] The greater deviation from idealized square pyramidal geometry in **1** promotes stronger overlap between adjacent magnetic d_{x2-y2} orbitals, fostering antiferromagnetic coupling. In this case, the O−Cu−O angles in **1** are slightly wider than those in **2**. One of the two crystallographically distinct Cu−O−Cu angles in **2** is larger than that in **1**, while the other is virtually identical. In addition, while the $\{Cu_2O_2\}$ units in **2** are restricted to being coplanar by the crystallographic symmetry, there is some small deviation from planarity (±0.003 and 0.004 Å) in the $\{Cu_2O_2\}$ units in **1**. While some empirical rules have been developed for the prediction of antiferromagnetism or ferromagnetism in $\{Cu_2(OH)_2\}$ rhomboid units,[32] these may not necessarily be germane to the specific copper phthalate system under study.

$$\chi_m T = \left(\frac{Ng^2\beta^2}{3k}\right)\left\{1 + \left[\frac{1}{3}\exp(J/kT)\right]\right\}^{-1} \qquad (1)$$

TGA and Gas Absorption Studies. According to TGA carried out under flowing N_2, compound **1** apparently lost its cocrystallized methanol molecules upon long-term storage (~60 days) at ambient temperature, as no appreciable mass loss occurred between 25 and ~210 °C (Figure S3 in the Supporting Information). At this latter temperature, the organic components of the structure were eliminated, as evidenced by a very significant and rapid mass loss. The 29.9% mass remnant at ~285 °C is consistent with the generation of $CuCO_3$ (30.0% calcd from desolvated **1**). The final mass remnant of 14.6% at 900 °C corresponds reasonably well with the deposition of copper metal (15.4% calcd).

Compound **2** underwent slow dehydration between 25 and ~220 °C, with a mass loss of 2.8%, matching that predicted for the elimination of 1 mol equiv of unligated water. Rapid expulsion of organics occurred at this temperature. The final mass remnant of 24.9% corresponds extremely well with the deposition of CuO (24.7% calcd). The TGA trace for **2** is shown in Figure S4 in the Supporting Information. Unfortunately, compound **2** showed no uptake of either H_2 or N_2 at either 77 or 293 K, despite the trial of a wide variety of possible desolvation/degassing routines. Single crystals of **2** took on a dark-blue hue upon exposure to gaseous NH_3 but visually retained their needlelike morphology. However, powder X-ray diffraction studies indicated a loss of crystallinity, revealing the likely destruction of the coordination polymer network as the ammonia molecules ligated to the divalent copper ions at the expense of dpa and/or pht ligands.

Conclusions

Kinked, hydrogen-bonding-capable dipyridine ligands, in tandem with *o*-dicarboxylate phthalate tethers, have permitted the construction of topologically novel divalent copper coordination polymers built from helical subunits. Despite similar coordination environments at copper in both **1** and **2**, striking differences in the overall coordination polymer dimensionalities and topologies are fostered by variances in the tethering length of the dpk and dpa ligands. The shorter tethering dpk moieties produce 3-fold helical motifs that organize with alternating chirality and are bridged through pht groups to create a mathematically predicted, but chemically unique, achiral 8-connected

(31) Pasan, J.; Delgado, F. S.; Rodriguez-Martin, Y.; Hernandez-Molina, M.; Ruiz-Perez, C.; Sanchiz, J.; Lloret, F.; Julve, M. *Polyhedron* **2003**, *22*, 2143–2153.

(32) Crawford, W. H.; Richardson, H. W.; Wasson, J. R.; Hodgson, D. J.; Hatfield, W. E. *Inorg. Chem.* **1976**, *15*, 2107–2110.

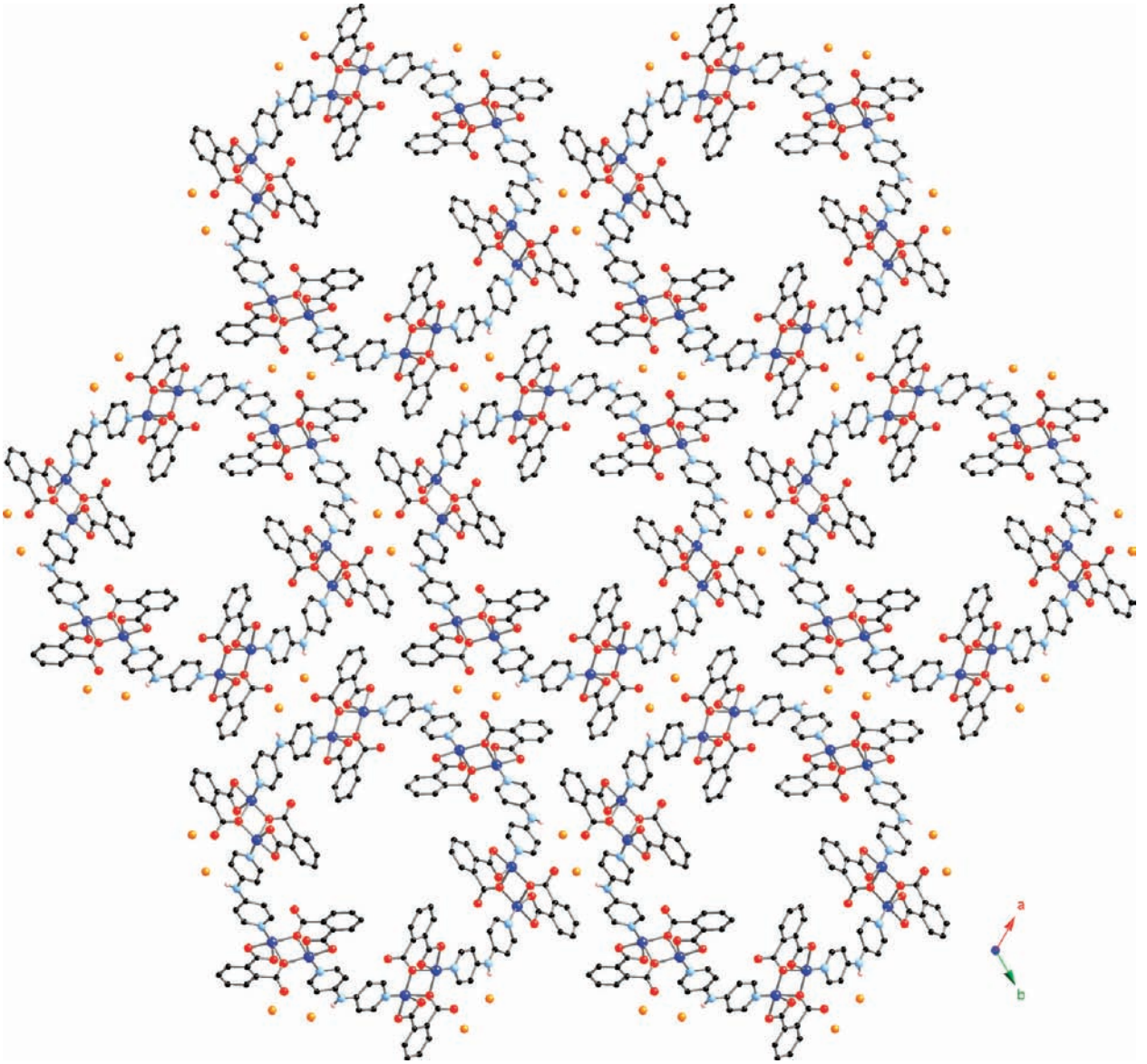

Figure 7. Stacking of $[Cu_2(pht)_2(dpa)]_n$ homochiral nanobarrels in **2**. Interstitial water molecules of crystallization are shown as orange spheres.

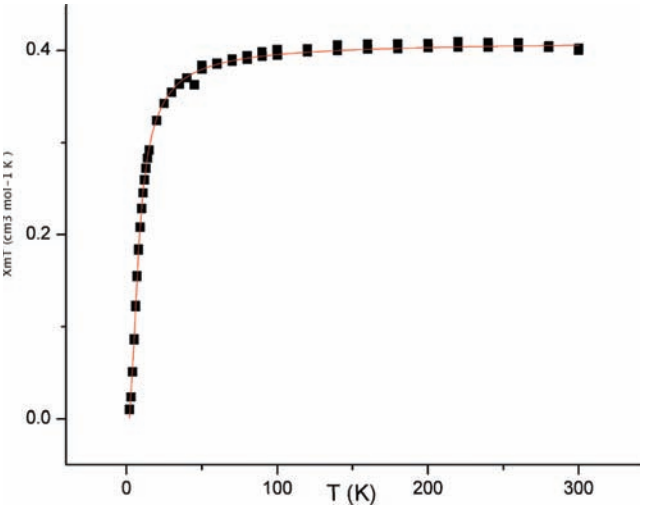

Figure 8. $\chi_m T$ vs T plot for **1**. The thin red line is the best fit to eq 1.

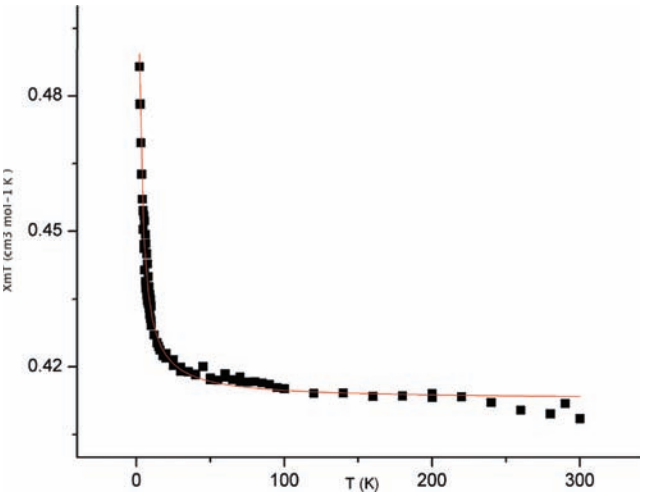

Figure 9. $\chi_m T$ vs T plot for **2**. The thin red line is the best fit to eq 1.

3D network. In contrast, the slightly longer, yet less sterically bulky, dpa ligands assist in the formation of homochiral 6-fold septuple helices, which are connected into aesthetic 1D coordination polymer nanobarrels through pht linkages. The decoration of the interior void spaces of the nanobarrels with hydrophobic aromatic rings prevents polar solvent occlusion during self-assembly and possibly gas absorptive behavior as well. While both **1** and **2** contain $\{Cu_2O_2\}$ rhomboid units with phthalate oxygen atoms bridging axial and equatorial coordination sites, subtle variances in coordination environment and d_{x2-y2} orbital overlap result in widely disparate magnetic superexchange behavior (antiferromagnetic in **1** and ferromagnetic in **2**). The unique highly connected topology of **1** portends a structurally rich coordination polymer chemistry for the underutilized dpk ligand; efforts in this direction are currently underway in our laboratory.

Acknowledgment. The authors gratefully acknowledge Michigan State University for financial support of this work. The thermogravimetric analyzer at King's College was purchased with a grant from the Alden Trust. We thank Dr. Rui Huang for elemental analysis, Dr. Reza Loloee for assistance with the SQUID magnetometer, and Dr. Wayne Ouellette of Syracuse University for gas absorption attempts with compound **2**.

Supporting Information Available: Hydrogen-bonding distances and structures for **2** and selected bond distances and angles, TGA traces, and crystallographic data in CIF format for **1** and **2**. This material is available free of charge via the Internet at http://pubs.acs.org. Crystallographic data in CIF format for **1** and **2** have also been deposited with the Cambridge Crystallographic Data Centre with Nos. 702152 and 702153, respectively. Copies of the data can be obtained free of charge via the Internet at http://www.ccdc.cam.ac.uk/conts/retrieving.html.